

EgoAdapt: Enhancing Robustness in Egocentric Interactive Speaker Detection Under Missing Modalities

XINYUAN QIAN*, School of Computer and Communication Engineering, University of Science and Technology Beijing, China

XINJIA ZHU*, MIIT Key Laboratory of Pattern Analysis and Machine Intelligence, College of Computer Science and Technology, Nanjing University of Aeronautics and Astronautics, China

ALESSIO BRUTTI, Fondazione Bruno Kessler, Italy

DONG LIANG[†], MIIT Key Laboratory of Pattern Analysis and Machine Intelligence, College of Computer Science and Technology, Shenzhen Research Institute, Nanjing University of Aeronautics and Astronautics, China

Talking to Me (TTM) task is a pivotal component in understanding human social interactions, aiming to determine who is engaged in conversation with the camera-wearer. Traditional models often face challenges in real-world scenarios due to missing visual data, neglecting the role of head orientation, and background noise. This study addresses these limitations by introducing **EgoAdapt**, an adaptive framework designed for robust egocentric ‘Talking to Me’ speaker detection under missing modalities. Specifically, EgoAdapt incorporates three key modules: (1) a **Visual Speaker Target Recognition (VSTR)** module that captures head orientation as a non-verbal cue and lip movement as a verbal cue, allowing a comprehensive interpretation of both verbal and non-verbal signals to address TTM, setting it apart from tasks focused solely on detecting speaking status; (2) a **Parallel Shared-weight Audio (PSA)** encoder for enhanced audio feature extraction in noisy environments, and (3) a **Visual Modality Missing Awareness (VMMA)** module that estimates the presence or absence of each modality at each frame to adjust the system response dynamically. Comprehensive evaluations on the TTM benchmark of the Ego4D dataset demonstrate that EgoAdapt achieves a mean average precision (mAP) of 67.39% and an accuracy (Acc) of 62.01%, significantly outperforming state-of-the-art method by 4.96% in Acc and 1.56% in mAP.

CCS Concepts: • **Human-centered computing** → **Human computer interaction (HCI)**.

Additional Key Words and Phrases: Interactive Speaker Identification, Multimodal Learning, Egocentric Video Understanding

ACM Reference Format:

Xinyuan Qian, Xinja Zhu, Alessio Brutti, and Dong Liang. 2026. EgoAdapt: Enhancing Robustness in Egocentric Interactive Speaker Detection Under Missing Modalities. 1, 1 (March 2026), 22 pages. <https://doi.org/10.1145/3797029>

*Both authors contributed equally to this research.

[†]Corresponding author.

This work is supported in part by the National Natural Science Foundation of China under grants 62272229 and 62306029, Shenzhen Science and Technology Program JCYJ20230807142001004, Beijing Natural Science Foundation (L233032) and Young Elite Scientists Sponsorship Program of the Beijing High Innovation Plan.

Authors’ Contact Information: Xinyuan Qian, School of Computer and Communication Engineering, University of Science and Technology Beijing, Beijing, China, qianxy@ustb.edu.cn; Xinja Zhu, MIIT Key Laboratory of Pattern Analysis and Machine Intelligence, College of Computer Science and Technology, Nanjing University of Aeronautics and Astronautics, Nanjing, China, xinjiazhu@nuaa.edu.cn; Alessio Brutti, Fondazione Bruno Kessler, Trento, Italy, brutti@fbk.eu; Dong Liang, MIIT Key Laboratory of Pattern Analysis and Machine Intelligence, College of Computer Science and Technology, Shenzhen Research Institute, Nanjing University of Aeronautics and Astronautics, Nanjing, China, liangdong@nuaa.edu.cn.

Permission to make digital or hard copies of all or part of this work for personal or classroom use is granted without fee provided that copies are not made or distributed for profit or commercial advantage and that copies bear this notice and the full citation on the first page. Copyrights for components of this work owned by others than the author(s) must be honored. Abstracting with credit is permitted. To copy otherwise, or republish, to post on servers or to redistribute to lists, requires prior specific permission and/or a fee. Request permissions from permissions@acm.org.

© 2026 Copyright held by the owner/author(s). Publication rights licensed to ACM.

Manuscript submitted to ACM

Manuscript submitted to ACM

1

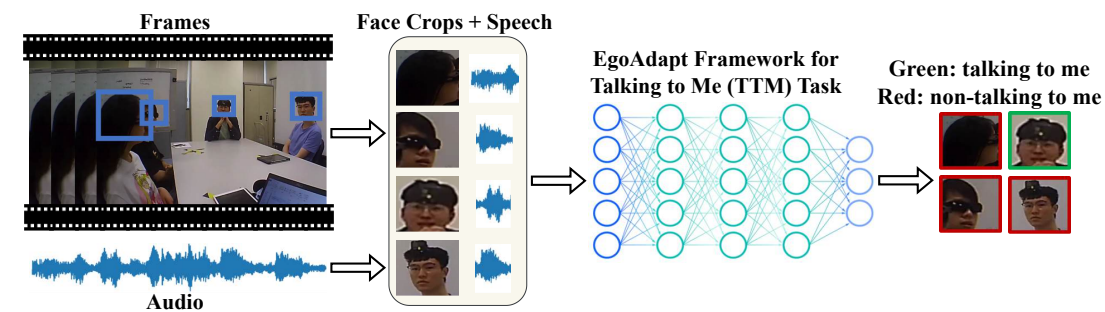
1 INTRODUCTION

Understanding social interactions is crucial for embodied agents in analyzing the intricate mechanisms behind human communications. Traditional social interaction methods mainly use speech signals, where advances in speech separation and extraction [30, 40, 47, 63], automatic speech recognition (ASR) [8, 32, 42, 66, 74], and dialog management [10, 11, 25] have improved the model’s ability to process and understand verbal communications. However, these auditory methods encounter considerable challenges, especially in complex multi-speaker scenarios. For example, speech separation approaches often struggle to robustly determine the number of speakers and attribute speech to the correct person [41, 55, 64]. When people speak simultaneously, it is also difficult for ASR models to recognize the spoken content of each individual [33, 34, 54]. Thus, it is important to introduce a front-end module to determine when, what, and to whom to respond. In contrast to auditory methods, vision-based methods [23, 56, 62] are immune to background noise or overlapping speech, offering a distinct advantage in environments where auditory signals are obscured. In particular, visual cues are beneficial when multiple conversations co-occur or in difficult noise situations, which can providing clarity and focus on non-verbal aspects of communication, such as facial expressions [1, 12, 21, 36], gaze estimation [14, 31, 67, 68, 75], head pose estimation [19, 45, 46, 50, 53], and body language [6, 43, 48, 51]. Despite these advances, visual methods also have limitations, particularly in distinguishing between relevant social cues and other facial or mouth movements, such as eating, yawning, or making emotional expressions. These unrelated motions can be mistakenly interpreted as meaningful social signals, which eventually affect the accuracy of visual interaction interpretation.

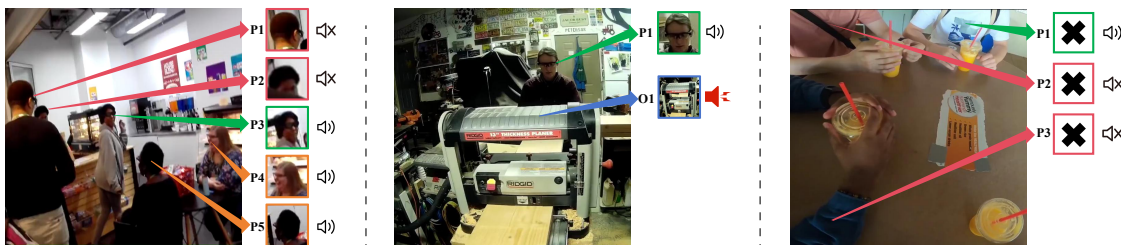
There has been a growing interest in combining audio-visual strengths to overcome the unimodal limitations to gain a more comprehensive understanding of social interactions. The TTM task, introduced along with the Ego4D dataset [22], determines which person is talking to the camera wearer given the synchronized audio-visual streams, as illustrated in Fig. 1 (a). While previous TTM methods [22, 37, 73] mainly focus on the exploration of different audio-visual fusion strategies, we particularly tackle realistic challenges, as illustrated in Fig. 1 (b)-(d). We consider the following realistic challenges: (1) Multi-Speaker Scenario: It is crucial to initially evaluate the individual’s speech initiation and subsequently assess the speaker’s head orientation to determine if they are talking to the camera wearer. The integration of audio and visual cues is pivotal for this assessment. (2) Background Noise Scenario: Existing methods make it difficult to distinguish speakers under intense background noise, which may lead to false or missed detection of the speaker. (3) Occluded Heads Scenario: In situations where the camera’s movement restricts the field of view, identifying the speaker becomes more challenging. Consequently, reliance on auditory cues becomes essential. Without visual indicators, audio signals can be analyzed to determine if someone is speaking toward the camera wearer.

To address the aforementioned challenges, we propose EgoAdapt, a novel method to enhance robustness in egocentric interactive speaker detection under missing modalities. To sum up, our contributions can be summarized as follows:

- Visual Speaker Target Recognition (VSTR) module for complex social cues: To better interpret speaker intent, the VSTR module integrates head orientation (non-verbal cue) and lip movement (verbal cue) as essential social signals. This approach allows EgoAdapt to more accurately determine when a speaker is directly addressing the camera wearer, making it suitable for complex social interactions rather than simple speaking-status detection.
- Parallel Shared-weight Audio (PSA) encoder for noise-resilient audio processing: EgoAdapt includes a specialized PSA encoder, which enhances the model’s ability to extract salient audio features even under substantial background noise.



(a) The TTM Task Setting



(b) Multi-Speaker Scenario

(c) Background Noise Scenario

(d) Ocluded Heads Scenario

Fig. 1. TTM task setting and challenges. (a) The TTM task consists in the frame-level identification of which person is talking to the camera wearer, given the synchronized audio-visual streams from the first-person perspective. (b)-(d) An overview of various real-life scenarios depicted in the egocentric video. (The red bounding box denotes a non-speaking person; the green bounding box denotes a person who is talking to the camera wearer; the blue bounding box denotes a sound source other than humans; the orange bounding box denotes a person who is talking but not talking to the camera wearer; the box with a cross indicates that no face was detected).

- Visual Modality Missing Awareness (VMMA) module for dynamic modality adaptation: We introduce a VMMA module, which dynamically assesses the presence or absence of head information in each frame. This module enables EgoAdapt to adjust its reliance on audio or visual cues based on real-time data availability, ensuring robust performance even in scenarios with occluded or absent visual head data.
- Experimental results show that our method achieves competitive performance on the TTM benchmark of the Ego4D dataset, surpassing existing baseline methods.

2 RELATED WORK

Egocentric video understanding is essential for applications such as human–robot interaction and assistive technologies, yet it faces unique challenges from camera motion, occlusion, and dynamic social settings. The TTM task aims to determine whether a visible participant addresses the camera wearer by leveraging multimodal cues from head pose, lip motion, and audio. Real-world conditions often introduce missing or degraded modalities, such as noisy speech, visual occlusion, or audio–visual misalignment. These challenges demand robust multimodal fusion methods capable of adapting to incomplete or corrupted inputs. This motivates the exploration of technologies that integrate discriminative features across modalities while ensuring resilience to modality loss.

2.1 Audio-Visual Active Speaker Detection

Audio-visual active speaker detection is a technique for identifying speakers that appear in synchronized audio-visual streams [52, 58, 71]. It determines the position and identity of speakers by analyzing the sound characteristics in audio or video signals, such as spectrum, sound intensity, and time-domain characteristics. The detection of audio and video speakers is commonly used in applications such as speech recognition [2, 35, 38, 65], audio processing [39, 44, 79], and video surveillance [17, 24, 61], which can help the system identify and separate different sources of sound with greater accuracy. The extended UniCon [76] introduced a spatial context to obtain a robust model by integrating three types of contextual information. In contrast, TalkNet [57] achieved better performance using cross-attention and self-attention modules to aggregate audio and visual features. Subsequently, based on this work, ASD-Transformer [15] improved the performance by introducing positional encoding and improving the attention module. To better exploit the potential of the attention module, ADENet [70] introduced multi-modal layer normalization to alleviate the distribution misalignment of audio-visual features. Despite these advances, existing audio-visual active speaker detection methods typically assume that both modalities are complete and of high quality, limiting their robustness in realistic egocentric scenarios where audio can be corrupted by environmental noise, visual cues (e.g., lip motion) may be occluded, and cross-modal synchronization may be imperfect. Moreover, most prior approaches focus on generic speaker detection and do not explicitly address the “Talking-to-Me” addressee recognition problem, which requires fine-grained modeling of interactions between the camera wearer and surrounding speakers.

2.2 Audio-Visual Social Interaction

Audio-visual social interaction refers to the simultaneous involvement of multiple different communication modes in social interaction, such as language, facial expressions, gestures, actions, etc. This multimodal social interaction can provide richer and more natural information for human-computer interaction and machine learning [9, 20, 72]. The TTM task is a specific application scenario proposed in the Ego4D dataset [22], which involves identifying whether someone is talking to the camera wearer in a video. It requires the model to not only analyze visual information in the video (such as head posture, facial expressions) but also combine auditory information (such as speaking voice, speech features). Ego4D baseline for TTM [22] introduces a method that utilizes ResNet-18 [26] for extracting facial features and ResNet-SE [29] for obtaining audio embeddings. The audio and video embeddings are subsequently concatenated and fed into a fully connected layer to predict the TTM task. Subsequently, based on this work, EgoT2 [73] refines the outputs from multiple models, each optimized for distinct tasks. QuAVF [37] proposes two separate models to process input videos and audio. In addition, it uses a facial quality score derived from a facial landmark prediction model to filter noisy face input data and integrates results from the two branches. Ex2Eg-MAE [60] proposes a novel framework leveraging novel-view face synthesis for dynamic perspective data augmentation from abundant exocentric videos and enhances self-supervised learning process for VideoMAE [59].

Unlike traditional speaker detection tasks that operate in static or controlled environments, egocentric detection deals with first-person, dynamic viewpoints, often involving abrupt camera movements, partial occlusions, and challenging background noise. Previous egocentric interactive speaker detection methods have primarily focused on audio-visual active speaker detection without delving into the effectiveness of the interaction between verbal and non-verbal cues for the interaction with the camera wearer. Moreover, the diverse nature of egocentric interaction scenarios often involves background noise interference in real-world settings. Furthermore, although some studies [22, 37] have acknowledged the issue of missing visual data, they have not addressed how to improve the model robustness against modality loss.

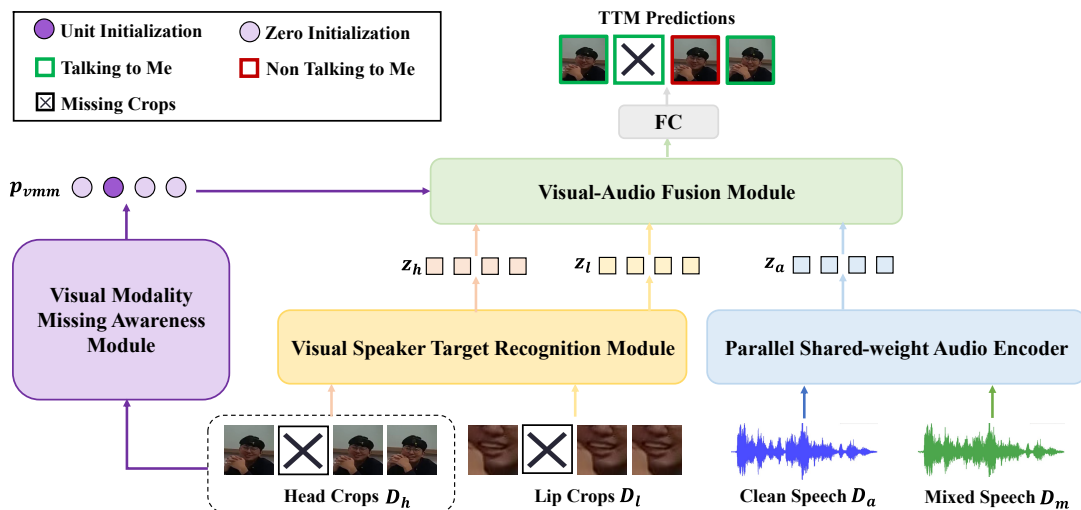


Fig. 2. Overview of the **EgoAdapt** framework for egocentric interactive speaker detection. The Visual Modality Missing Awareness (VMMA) module assesses modality availability and outputs p_{vmm} to guide adaptation. The Visual Speaker Target Recognition (VSTR) module extract non-verbal and verbal cues (z_h and z_l) from head crops D_h and lip crops D_l , respectively, while the Parallel Shared-weight Audio (PSA) encoder processes clean and noisy audio (D_a and D_m) to produce z_a . These cues are fused in the Visual-Audio Fusion module for the final TTM Prediction of "Talking to Me" or "Non Talking to Me".

Recognizing these limitations, our proposed EgoAdapt framework introduces a novel VMMA module that dynamically adjusts system responses based on the availability of visual and audio input, allowing it to handle missing visual data in real time. Furthermore, we incorporate a VSTR module that explicitly interprets head orientation as a non-verbal cue and lip movement as a verbal cue to improve the model's capability in distinguishing between multiple speakers in egocentric settings. As for body-part cues (e.g., hands and torso), while they may carry potentially rich information, they are often difficult to obtain reliably under the egocentric setting. Frequent occlusions, incomplete visibility, and motion blur from the moving camera severely undermine their consistency. In contrast, head and speech modalities remain relatively stable and controllable. For this reason, our current framework focuses on these more reliable signals to ensure robustness and reproducibility. By combining these modules with a PSA encoder designed to reduce noise interference, EgoAdapt offers a robust solution for the TTM task, effectively addressing the limitations of current audio-visual speaker detection approaches.

3 METHODOLOGY

3.1 Problem Definition and Method Overview

Given a synchronized audio-visual stream, we aim to determine whether a participant in a video frame is talking to the camera wearer or not. Specifically, we define head crops $D_h = \{h_t\}_{t=1}^T$ as the head of the detected speaker in each frame where $t = 1, \dots, T$ with T the total frame number and lip crops $D_l = \{l_t\}_{t=1}^T$ as the extracted lip region. The corresponding audio segments are denoted as $D_a = \{a_t\}_{t=1}^T$ and the TTM problem can be formulated as:

$$\hat{y}_t = \mathcal{F}(D_h, D_l, D_a | \Omega) \quad (1)$$

where $\mathcal{F}(\cdot)$ denotes the neural network with trainable parameters Ω . \hat{y}_t is the estimate of TTM label y_t that is set to 1 if the participant in frame t is talking to the camera wearer and 0 otherwise.

Our proposed EgoAdapt framework is shown in Fig. 2. In particular, our framework addresses three key challenges in egocentric audio-visual data processing:

(Q1) How can visual information be used to learn non-verbal cues for accurately identifying the person talking to the camera wearer? To determine if someone is talking to the camera wearer, we use the VSTR module to extract head orientation and lip features, capturing both non-verbal and verbal cues from video frames (Section 3.2).

(Q2) How can the TTM task be addressed in noisy environments? To maintain the system robustness, the proposed PSA encoder processes both clean and mixed audio segments using shared weights to handle variable noise levels, with the network trained on Mean Square Error (MSE) loss (Section 3.3).

(Q3) How can the framework cope with situations where the visual modality is sometimes missing? To tackle incomplete visual information, the VMMA module dynamically evaluates the availability of both visual and audio cues. It outputs p_{vmm} , which directs the model in adjusting to modality variations, ensuring stable performance even in the absence of visual cues (Section 3.4).

The Visual-Audio Fusion module then integrates features from all modules, allowing the system to produce accurate frame-level predictions of whether the person is "Talking to Me" even under severe acoustic conditions (Section 3.5).

3.2 Visual Speaker Target Recognition Module

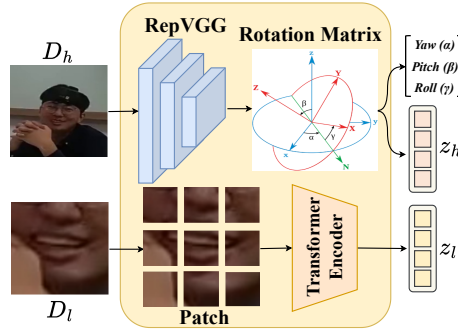


Fig. 3. Visual Speaker Target Recognition (VSTR) module. It includes two components: the Head Pose Feature Extraction Module, which captures head orientation (non-verbal cues), and the Lip Feature Extraction Module, which extracts lip movement features (verbal cues).

Our vision branch is designed to extract and analyze critical information about the speaker's participation. When an active speaker is detected, it is imperative to determine the speaking target, which identifies the individual or entity to whom the speaker is directing their speech. In typical interactive scenarios, as illustrated in Fig. 1 (b), there is a notable tendency to face-to-face orientation when the camera wearer is conversing with a speaker. Therefore, VSTR becomes particularly relevant to discover whether the speaker is talking to the camera wearer directly. As illustrated in Fig. 3, to simultaneously capture both the visual speaking features, e.g., lip motions and head orientations, our approach integrates two distinct modules within the visual branch to enhance the analysis of speaker engagement in TTM task.

3.2.1 Head Pose Feature Extraction Module. Our head pose feature extraction module follows the general 6D rotation representation proposed by Zhou et al. [77] and employs the RepVGG backbone [16] for efficient feature extraction.

Compared to these works, our contributions are twofold: (1) we integrate the 6D representation into the *EgoAdapt* pipeline for the TTM task, enabling head pose estimation to serve as an intermediate representation for multi-modal temporal reasoning; and (2) we adapt the feature extraction and normalization process to the egocentric setting, where head crops are obtained from continuous first-person video with varying scale and occlusion. In this way, our module extends [77] and [16] by embedding their strengths into a unified framework tailored for egocentric conversation understanding. As shown in Fig. 3, the goal of the head pose feature extraction module is to estimate the head orientation in three-dimensional space by computing the yaw (α), pitch (β), and roll (γ) angles based on the input head crops D_h . The first step is to normalize the image to ensure consistent scaling. This is achieved by computing $D_{h_{norm}} = \frac{D_h - \mu}{\sigma}$, where μ and σ are the mean and standard deviation of the training dataset, respectively. Next, the normalized image $D_{h_{norm}}$ is passed through the trained RepVGG model [16] for feature extraction, represented as:

$$F_h = \text{RepVGG}(D_{h_{norm}}; W_{\text{RepVGG}}) \quad (2)$$

where $F_h \in \mathbb{R}^{N_f}$ is the feature representation obtained from the model, and W_{RepVGG} are the model weights. To efficiently predict the head pose, a 6D rotation matrix representation is employed. Following the approach by Zhou et al. [77], the rotation matrix is reduced to a 6-dimensional representation by dropping the last column vector of the rotation matrix, ensuring that the orthogonality constraint is satisfied. This 6D representation, denoted g_{GS} , is given by:

$$A = g_{GS}(F_h) = \left(\begin{bmatrix} | & | & | \\ a_1 & a_2 & a_3 \\ | & | & | \end{bmatrix} \right) = \begin{bmatrix} | & | \\ a_1 & a_2 \\ | & | \end{bmatrix} \quad (3)$$

This 6D representation is then mapped back to the 3x3 rotation matrix, denoted by f_{GS} , using the following equation:

$$B = f_{GS}(A) = \left(\begin{bmatrix} | & | \\ a_1 & a_2 \\ | & | \end{bmatrix} \right) = \begin{bmatrix} | & | & | \\ b_1 & b_2 & b_3 \\ | & | & | \end{bmatrix} \quad (4)$$

The vectors b_1, b_2, b_3 are computed as follows:

$$\begin{aligned} b_1 &= \text{Norm}(a_1) = \frac{a_1}{\|a_1\|} \\ b_2 &= \text{Norm}(u_2) = \frac{u_2}{\|u_2\|}, u_2 = a_2 - (b_1 \cdot a_2) b_1 \\ b_3 &= b_1 \times b_2, \end{aligned} \quad (5)$$

where $\text{Norm}(\cdot)$ represents a normalization function using the L_2 -norm. The orthogonal features B are used to predict the head pose angles. This is done by applying a weight matrix $W_{out} \in \mathbb{R}^{3 \times 3N_f}$ and a bias $b_{out} \in \mathbb{R}^3$, leading to the

prediction of the pose angles $\theta = \begin{bmatrix} \alpha \\ \beta \\ \gamma \end{bmatrix}$. The regression equation is given by

$$\theta = W_{out} \cdot B + b_{out} \quad (6)$$

where α, β , and γ represent the yaw, pitch, and roll angles, respectively. Afterward, the predicted angles θ are converted into a rotation matrix R_p using the function $R_p = \text{EulerToRotationMatrix}(\theta)$. The final output is the predicted head pose angles $z_h = \theta$, which represent the head's orientation in three-dimensional space.

3.2.2 Lip Feature Extraction Module. Let $D_l \in \mathbb{R}^{H \times W \times C}$ denote the input image, where H and W are the height and width, and C is the number of channels (e.g., RGB). The image is partitioned into non-overlapping patches of size $P = 32$, resulting in $N = \frac{H \times W}{P^2}$ patches, each flattened into a vector $p'_i \in \mathbb{R}^{P^2 \times C}$. These flattened patches are then projected into a new feature space D via a linear projection matrix $W_p \in \mathbb{R}^{D \times P^2 \times C}$, yielding the patch representations z_i . To preserve spatial relationships between the image patches, positional encodings $P_i \in \mathbb{R}^D$ are added to each patch feature z_i . The final patch representation, after adding the positional encoding, is mathematically expressed as:

$$z_i^{\text{emb}} = z_i + P_i \quad (7)$$

where z_i is the feature vector and P_i is the positional encoding for the i -th patch. The sequence of positionally encoded patches is then represented as:

$$\mathbf{Z}^{\text{emb}} = [z_1^{\text{emb}}, z_2^{\text{emb}}, \dots, z_N^{\text{emb}}] \quad (8)$$

where $\mathbf{Z}^{\text{emb}} \in \mathbb{R}^{N \times D}$ is the matrix of positionally encoded patch features. To facilitate the extraction of global features, a special classification token $z_{\text{CLS}} \in \mathbb{R}^D$ is prepended to the input sequence. The modified input sequence, including the [CLS] token and the positionally encoded patch features, is represented as:

$$\mathbf{Z}^{\text{input}} = [z_{\text{CLS}}, z_1^{\text{emb}}, \dots, z_N^{\text{emb}}] \quad (9)$$

where z_{CLS} is the global feature token and each z_i^{emb} is the final encoded representation of the i -th patch after the addition of positional encodings. The output of the Transformer encoder is the matrix \mathbf{Z}^{enc} , defined as:

$$\mathbf{Z}^{\text{enc}} = \text{Transformer Encoder}(\mathbf{Z}^{\text{input}}) \quad (10)$$

where $\mathbf{Z}^{\text{enc}} \in \mathbb{R}^{(N+1) \times D}$ represents the processed sequence of patch features. The output corresponding to the [CLS] token, $z_{\text{CLS}}^{\text{out}}$, serves as the global feature vector z_l for the entire image. This global feature vector is defined as:

$$z_l = z_{\text{CLS}}^{\text{out}} \in \mathbb{R}^D \quad (11)$$

where $z_l \in \mathbb{R}^D$ represents the high-dimensional semantic representation of the image.

3.3 Parallel Shared-weight Audio Encoder

To enhance noise robustness, we propose a special audio encoder as shown in Fig. 4. Let $D_a(t)$ denotes the clean speech signal, $n(t)$ represents the additive noise, and $D_m(t)$ be the mixed speech, expressed as:

$$D_m(t) = (1 - \gamma) \cdot D_a(t) + \gamma \cdot n(t) \quad (12)$$

where γ is a weighting factor that controls the proportion of noise to clean speech. Then, clean speech D_a and mixed speech D_m are transformed into their respective Mel spectrograms: $S_a = \text{MelSpec}(D_a)$ and $S_m = \text{MelSpec}(D_m)$, where $\text{MelSpec}(\cdot)$ denotes the Mel spectrogram function that provides a time-frequency representation suitable for audio signal processing. The audio encoder f_{enc} operates on both the clean and mixed Mel spectrograms to derive latent embeddings $z_a = f_{\text{enc}}(S_a; \theta_a)$ and $z_m = f_{\text{enc}}(S_m; \theta_m)$ where θ_a and θ_m are the parameters of the encoder associated with clean and mixed speech, respectively. The shared loss function, \mathcal{L}_{MSE} , is defined as the squared Euclidean distance between the latent embeddings of clean and mixed speech (z_a and z_m), given by:

$$\mathcal{L}_{\text{MSE}} = \|z_a - z_m\|^2 \quad (13)$$

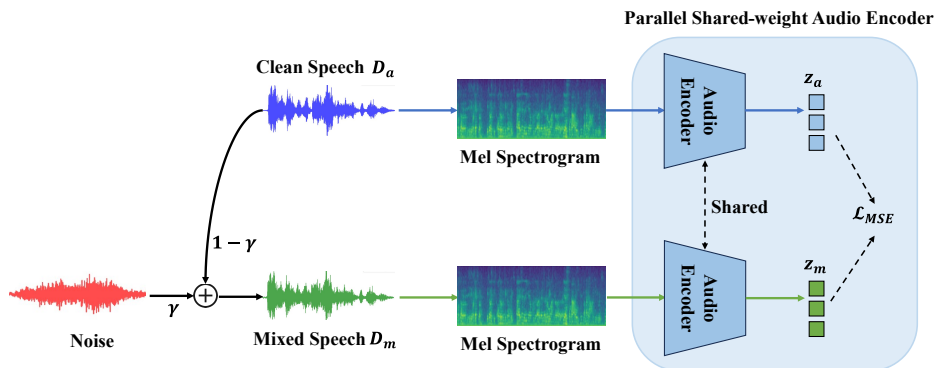


Fig. 4. Parallel Shared-weight Audio (PSA) encoder. It processes clean speech D_a and noise-mixed speech D_m (ratio γ) into Mel spectrograms, encodes them with shared weights to obtain embeddings z_a and z_m , and uses MSE loss to enforce noise-robust audio features.

This encourages the encoder to extract noise-robust features by training the model to learn representations from both clean and noisy inputs [7, 18], pushing the model to focus on the essential characteristics of the speech signal while disregarding noise components.

For audio encoder, we adopt the Whisper-small model [49], which has been pre-trained on over 680,000 hours of diverse speech data for automatic speech recognition (ASR) and speech translation tasks to encode the acoustic and semantic characteristics inherent in the speech input. Compared to other unsupervised speech pre-trained models like Wav2vec 2.0 [5] and HuBERT [28], Whisper’s output features are more closely aligned with different downstream tasks, making it an ideal choice for task transfer learning. Furthermore, the extensive training set of Whisper enhances its performance and generalizability. Therefore, we select it as the Audio encoder to generate a comprehensive feature vector, denoted as z_a .

3.4 Visual Modality Missing Awareness Module

The Visual Modality Missing Awareness (VMMA) module (Fig. 5), is designed to address the challenges associated with missing visual information i.e., Fig. 1 (c). The module processes two different inputs: head crops D_h , and p_{vmm} initialization. The inputs undergo a transformation into a Visual Mask Matrix that is dynamically updated to reflect the presence or absence of visual cues, which extracts both *coarse-grained* and *fine-grained* features.

3.4.1 Fine-grained. Firstly, our VMMA prompt $p_{vmm}^{b,t,d}$ is initialized to zero to establish a foundation for integrating modality-specific details into the model. In this context, b, t, d represents the batch size, frame number, and feature dimension. This initialization allows for dynamic adjustments during training, effectively managing instances where modalities are missing.

The fine-grained prompt $p_{vmm}^{b,t,d}$ focuses explicitly on the temporal dimension T by indicating whether specific frames are present or missing. If a head crop at t is present, $p_{vmm}^{b,t,d}$ is set to zero; otherwise $p_{vmm}^{b,t,d}$ takes a value of one during visual absence. This mechanism efficiently adjusts the values of tensor $p_{vmm}^{b,t,d}$ based on frame availability, significantly enhancing the model’s ability to manage and rectify missing modalities with precision.

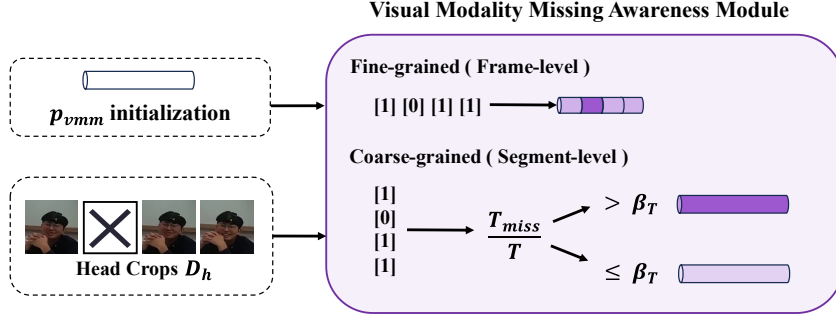


Fig. 5. Visual Modality Missing Awareness (VMMA) module dynamically handles missing visual inputs by processing head crops D_h and the initialized prompt p_{vmm} . It extracts fine-grained features by tracking frame presence and coarse-grained features by quantifying the missing frame ratio Δ_c .

3.4.2 *Coarse-grained.* To quantify the absence of frames within a head crop, we introduce Δ_c , defined as the ratio of missing frames to the total frame number:

$$\Delta_c = \frac{T_{miss}}{T} \quad (14)$$

where T_{miss} represents the number of missing head crops and T is the total number of frames. By setting a threshold β_T to gauge the severity of missing data, $p_{vmm}^{b,t,d}$ is modified accordingly

$$p_{vmm}^{b,t,d} = \begin{cases} 1 & \text{if } (\Delta_c < \beta_T \text{ and } (d \leq \frac{D}{2})) \text{ or } (\Delta_c \geq \beta_T \text{ and } (d > \frac{D}{2})) \\ 0 & \text{otherwise} \end{cases} \quad (15)$$

This formula delineates how $p_{vmm}^{b,t,d}$ is assigned a value of 1 or 0 in different segments of the feature dimension D , depending on whether the proportion of missing frames Δ_c falls below or exceeds the threshold β_T . Specifically, when the proportion of missing data is less than β_T , the first half of the feature dimensions is activated (set to 1), while the second half is deactivated (set to 0). In contrast, when the proportion of missing data surpasses β_T , the first half is deactivated and the second half is activated. This adaptive mechanism enables the model to effectively respond to varying levels of missing data in video frames.

To enhance the VMMA module effectiveness, we propose a dynamic design for the threshold β_T , which is adaptable based on the data context and the operational environment. It can be fine-tuned using a validation dataset, allowing the model to learn from previous instances of missing data. The adaptive threshold is formulated as

$$\beta_T = \text{mean}(\Delta_c) + k \cdot \text{std}(\Delta_c) \quad (16)$$

where k is a tunable parameter that adjusts the sensitivity of the threshold based on the distribution of missing data across different scenarios.

3.5 Visual-Audio Fusion Module

In the TTM task, integrating information from different modalities can be carried out in various stages. Among existing methods, the Ego4D baseline for TTM [22] and EgoT2 [73] employed feature-level fusion in which the extracted features of each modality (e.g., visual and audio) are fused early, before being input to a shared classification model.

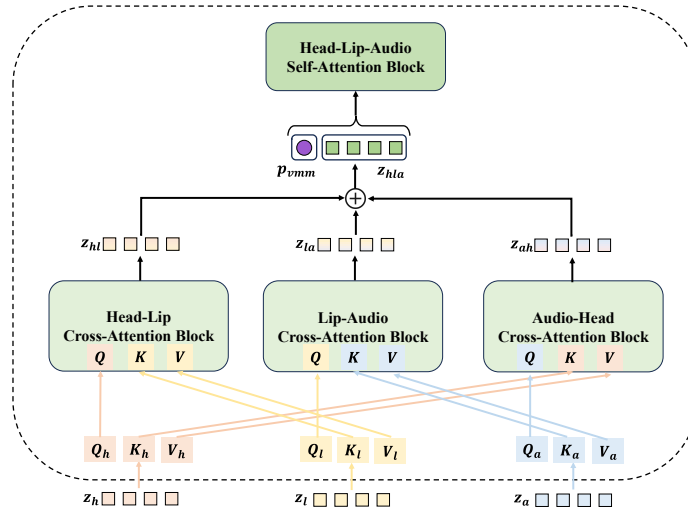


Fig. 6. Overview of Visual-Audio Fusion module. It fuses head pose z_h , lip motion z_l , and audio z_a via Head-Lip, Lip-Audio, and Audio-Head cross-attention blocks. Aggregated features with VMMA prompt p_{vmma} are refined by self-attention for final “Talking to Me” prediction.

Although this fusion method allows the model to learn correlations between the modalities at the feature level, it can struggle with misaligned or noisy data. QuAVF [37] applied decision-level fusion in which each modality has its own classification model, and the results of each model are combined to make the final decision. This fusion method is more robust to errors in individual modalities but may miss fine-grained interactions. We considered multiple possible fusion configurations among the three modalities. The chosen design (Head-Lip, Lip-Audio, Audio-Head) was motivated by (i) physiological and conversational relevance (lip motion tightly couples with audio; head pose naturally correlates with both speech rhythm and lip dynamics), and (ii) empirical performance. Alternative pairings such as Lip-Head or Audio-Lip-Head chains were tested in preliminary experiments but showed marginal or redundant gains compared with the selected combination. Hence, we retained the current setup as a balanced trade-off between model complexity and effectiveness.

As illustrated in Fig. 6, we propose a Visual-Audio Fusion module that integrates multi-modal inputs derived from three primary sources: 1) the head pose feature extraction module, which generates the head features represented as z_h ; 2) the lip feature extraction module, which produces the lip features denoted as z_l and 3) the PSA encoder, which extracts audio features represented as z_a . Following the generation of the input features, the module employs specially designed two-by-pair interactive cross-attention mechanisms to enhance the interactions between modalities. We illustrate this using the head-lip cross-attention block as an example. In this block, the head features z_h are used as queries Q , while the lip features z_l serve as keys K and values V . The attention mechanism is computed as follows

$$z_{hl} = \text{Softmax} \left(\frac{Q_h K_l^T}{\sqrt{d_k}} \right) V_l \quad (17)$$

where d_k represents the key vectors’ dimensionality, the softmax function normalizes the attention scores. The resulting output z_{hl} encapsulates the enhanced representation of head and lip interactions. Similarly, the lip-audio cross-attention

block and the audio-head cross-attention block are constructed using the same principles. For the Lip-Audio Cross-Attention block, lip features z_l are used as queries, while audio features z_a are used as keys and values, resulting in output z_{la} . For the Audio-Head Cross-Attention block, the audio features z_a serve as queries, the head features z_h acting as keys and values, resulting in the output z_{ah} . The outputs from the three cross-attention blocks, z_{hl} , z_{la} , and z_{ah} , are then aggregated through an addition operation to form a unified representation

$$z_{hla} = z_{hl} + z_{la} + z_{ah} \quad (18)$$

The aggregated representation z_{hla} is concatenated with the output p_{vmm} obtained from the VMMA module. This concatenated representation is then fed into the Head-Lip-Audio Self-Attention block, which further processes the combined information. This output culminates in the TTM prediction results, enabling a comprehensive understanding of the multi-modal interactions.

4 EXPERIMENTATION, RESULT AND ANALYSIS

4.1 Datasets

We conducted our experiments using the Ego4D social interaction benchmark [22], a pivotal dataset in social interaction research that captures complex, real-world interactions from an egocentric perspective. This dataset comprises 389 training clips, amounting to approximately 32.4 hours of footage, making it suitable for training models to recognize and interpret social cues in dynamic environments. It includes 50 validation clips with around 4.2 hours and 133 test clips totaling 11.1 hours. The video data are recorded at a frame rate of 30 frames per second, while the audio is sampled at 16 kHz, ensuring high-quality input for our analysis.

To enhance the noise robustness of our system, we selected the WHAM! dataset [69] as the source of noise data. This dataset is crucial for assessing the model’s performance in real-world scenarios, as it consists of noisy mixtures generated by combining speech from the WSJ0-2mix corpus with real-world noise recordings, providing approximately 42 hours of noisy speech data. This diversity in noise conditions is essential for training robust models capable of performing well in varied auditory environments. To adapt this dataset to our task, we randomly select a noise sequence from the WHAM! dataset with a 50% probability and add it to the original clean speech, thereby creating mixed speech for training purposes. We also experimented with various signal-to-noise ratios (SNR) ranging from -10 to 10 dB to evaluate performance under different noise conditions.

4.2 Baselines

We compare with four representative methods:

- (1) Random Guess [22]: outputs two-label predictions via Bernoulli sampling.
- (2) ResNet-18 Bi-LSTM [22]: extracts facial and audio embeddings with ResNet-18 and ResNet-SE, concatenates them, and predicts TTM with a fully-connected layer.
- (3) EgoT2 [73]: refines outputs from models trained for separate tasks.
- (4) QuAVF [37]: filters data via face quality scores, encodes visual/audio features with ResNet-50 [26] and Whisper [49], and applies quality-aware fusion.

All methods are evaluated under identical parameter settings.

Table 1. Head pose feature extraction parameters.

Parameter	Head Pose Feature Extraction
Backbone Model	6DRepNet
Pretrained	Yes (frozen weights)
Deploy Mode	True
Input Feature	224x224 pixels image
Pooling Layer	Adaptive Average Pooling
Output Dimension	6 (Ortho6D Representation)
Rotation Matrix Computation	Ortho6D to Rotation Matrix
Euler Angles Computation	Rotation Matrix to Euler Angles
Training Dataset	300W-LP

Table 2. Lip and audio feature extraction parameters.

Parameter	Lip Feature Extraction	Audio Feature Extraction
Backbone Model	CLIP ViT-B/32	Whisper-small
Pretrained	Yes (frozen weights)	Yes (frozen weights)
Input Feature	224x224 pixels image	Log-Mel Spectrogram
Embedding Dimension	512	768
Temporal Module Dimension	128	128
Number of Temporal Layers	1	1
Number of Attention Heads	8	8
Max Temporal Length	900	1500
Position Embedding	Learnable, max length: 900	Learnable, max length: 1500
Classification Token (CLS)	Yes	N/A
Dropout	0	0.25

4.3 Evaluation Metrics

Following previous works [22, 37, 73], we use the mAP, which measures the precision-recall trade-off, and Top-1 accuracy, which indicates the proportion of correctly predicted top-ranking results, as evaluation metrics (the higher value corresponds to better results). Unless otherwise specified, we conduct comparative experiments in the test set and the validation set, while ablation experiments are performed on the validation set.

4.4 Backbones

4.4.1 Head Pose Feature Extraction. According to Table 1, we use 6DRepNet [27] with frozen pretrained weights for head pose estimation. The model runs in deploy mode on 224x224 images, applies adaptive average pooling, and outputs a 6D Ortho6D representation [3, 4]. Rotation matrices are computed from Ortho6D and converted to Euler angles. The backbone is trained on the 300W-LP dataset [78].

4.4.2 Lip Feature Extraction. As shown in Table 2, we use CLIP Vision Transformer (ViT)-B/32 [49] to encode 224x224 lip images into 512-d features. A temporal module (dim 128, 1 layer, 8 heads) processes sequences of up to 900 frames with learnable position embeddings and a CLS token. No dropout is applied.

4.4.3 Audio Feature Extraction. As shown in Table 2, we use Whisper-small [49] to encode log-Mel spectrograms into 768-d features. The temporal module matches the lip branch but handles sequences up to 1500 frames.

Table 3. Comparison of our proposed EgoAdapt with existing methods on TTM benchmark of Ego4D dataset.

Method	Val		Test	
	Acc(%)	mAP(%)	Acc(%)	mAP(%)
Random Guess [22]	33.44	53.82	47.41	50.16
ResNet-18 Bi-LSTM [22]	64.31	56.50	49.75	55.06
EgoT2 [73]	66.07	60.80	56.17	57.82
QuAVF [37]	71.80	71.20	57.05	65.83
Ours	81.14	84.83	62.01	67.39

Table 4. Comparison of the performance for different modality and backbone combinations.

Modality	Visual Backbone	Audio Backbone	Acc(%)	mAP(%)
V	ViT [49]	\times	67.25	62.51
A	\times	Whisper [49]	75.64	77.55
V, A	ViT	WavLM [13]	72.69	72.96
V, A	TalkNet [57]	WavLM	72.52	72.59
V, A	TalkNet	Whisper	73.65	77.51
V, A	ViT	Whisper	75.33	77.21

4.5 Training Settings

We train with Adam ($\text{lr } 1 \times 10^{-5}$) and Focal Loss ($\gamma = 2, \alpha = 0.25$). Training runs for 40 epochs with gradient clipping (1.0) and early stopping (patience 100). Batch size is 1 with 4 data loader workers. Head and lip images are resized to 224×224 ; audio is represented by 80-d log-Mel features (25 ms window, 10 ms hop, 16 kHz). Noise augmentation (ratio 0.5) uses WHAM! noise with 50% probability. A coarse-grained prompt type (threshold 0.2) is adopted. Cross-attention has 6 randomly initialized multi-head layers (8 heads each); self-attention [57] has 1 layer with 8 heads.

4.6 Comparison with the State-of-the-art

The experimental results are presented in Table 3. Previous approaches such as Random Guess [22] and ResNet-18 Bi-LSTM [22] focus mainly on basic classification tasks and simple fusion of multimodal data. These methods either ignore or inadequately leverage the intricate cooperation between audio and visual modalities, which is crucial for a more comprehensive understanding of egocentric video content. For example, Random Guess achieves only 47.41% Acc and 50.16% mAP on the test set, while ResNet-18 Bi-LSTM slightly improves the results to 49.75% Acc and 55.06% mAP, yet still falls short in handling the complex interplay between modalities. While some methods, such as EgoT2 [73] and QuAVF [37], attempt to incorporate both audio and visual signals, they have poor performance compared to EgoAdapt. Specifically, EgoT2 achieves 55.93% Acc and 57.51% mAP on the test set, while QuAVF reaches 57.05% Acc and 65.83% mAP. However, these methods are primarily designed for tasks involving trimmed short videos, limiting their ability to model long-range dependencies and interactions necessary for egocentric interactive speaker detection. QuAVF, despite its reasonable results, has constrained performance due to its reliance on static quality filtering and less dynamic fusion strategies. Our proposed EgoAdapt outperforms all the comparison methods with the highest scores in both the validation set (77.40% Acc, 79.37% mAP) and the test set (61.95% Acc, 66.75% mAP). As a result, EgoAdapt sets a new benchmark in egocentric interactive speaker detection, outperforming all previous methods by a significant margin.

Table 5. The effects of different VMMA module settings on the validation set. β represents an adaptive parameter trained to optimize the model’s performance under the Coarse-Grained setting. (Bold: best results)

p_{vmm}	Threshold (β_T)	Acc (%)	mAP (%)
None	\times	77.40	79.37
Fine-Grained	\times	81.66	84.53
Coarse-Grained	β	81.14	84.83
	20%	80.29	84.07
	50%	78.18	83.73
	70%	78.01	83.50

Table 6. The effects of VSTR, PSA, and VMMA. (Bold: best results)

VSTR	PSA	VMMA	Acc(%)	mAP(%)
\times	\times	\times	75.33	77.21
\checkmark	\times	\times	78.31	82.60
\times	\checkmark	\times	77.26	80.15
\times	\times	\checkmark	78.36	82.44
\times	\checkmark	\checkmark	79.55	83.06
\checkmark	\times	\checkmark	80.67	83.82
\checkmark	\checkmark	\times	78.57	83.99
\checkmark	\checkmark	\checkmark	81.14	84.83

4.7 Ablation Study

4.7.1 Preliminary study on modality/backbone combinations. Before presenting our proposed Visual-Audio Fusion module, we first conduct preliminary experiments on different modality and backbone combinations, following the experimental setup of QuAVF [37] for unimodal and TalkNet [57] for multimodal. The results are summarized in Table 4. Notably, our results align with those reported in [37], as the unimodal A consistently outperforms the multimodal A+V, even when different backbone networks are employed. For example, when using the Whisper audio backbone for modality A, the unimodal performance achieves an Acc of 75.64% and an mAP of 77.55%. In comparison, the best performing multimodal combination (A+V with ViT visual backbone and Whisper audio backbone) results in an Acc of 75.33% and an mAP of 77.21%. The unimodal A outperforms the multimodal A+V by 0.31% in Acc and 0.34% in mAP. Additionally, the performance of the unimodal visual modality (V) is significantly lower than the unimodal audio modality (A). Specifically, the Acc of V with the ViT backbone is 67.25%, while the unimodal audio modality Whisper achieves 75.64%, an 8.39% increase in Acc. Even in multimodal combinations (V, A), such as ViT + Whisper, the performance is still inferior to the unimodal audio results, highlighting the limited contribution of the visual modality in this setup.

The above analysis suggests that, in this particular experimental setup, the addition of the visual modality does not provide a substantial advantage and, in some cases, may even slightly hinder performance. We identify two primary factors contributing to this phenomenon: (1) Data-related issues: Approximately one-third of the head crops in the dataset are missing, leading to incomplete visual data that impedes the model’s ability to effectively leverage visual features. (2) Model-related issues: Previous models primarily focused on identifying speaking states but did not delve into the specifics of the speaking target, resulting in misclassifications, particularly errors in labeling speakers who are not speaking to the camera-wearer. Our research seeks to address these challenges and provide a more effective A+V solution for the TTM task, with the potential to surpass the performance of the unimodal A approach. We use the A+V configuration with the ViT visual backbone and Whisper audio backbone as our baseline.

4.7.2 Effects of the VSTR, PSA, and VMMA. Table 6 presents the ablation results for the VSTR module, PSA encoder, and VMMA module. The full configuration with all three components achieves the best performance, reaching 81.14% accuracy and 84.83% mAP. When using partial configurations, VSTR+VMMA attains 80.67% / 83.82% (Acc / mAP), slightly outperforming PSA+VMMA (79.55% / 83.06%), indicating the importance of spatial-temporal reasoning in the fusion process. The lowest result (75.33% / 77.21%) is obtained when all three modules are removed. In this setting, the system relies solely on optimized backbone networks and the cross-modal fusion mechanism. Even under this

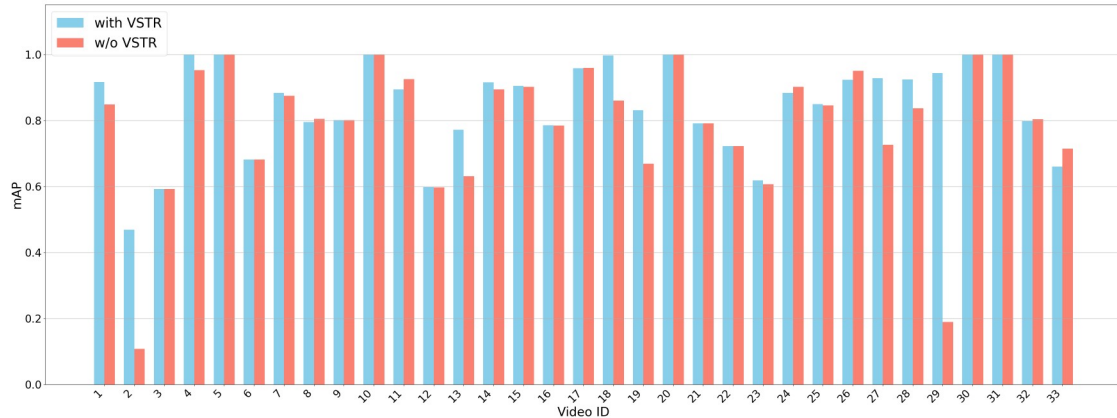


Fig. 7. Comparison of the performance with or w/o VSTR.

minimal configuration, the performance already surpasses QuAVF (Table 1) by a notable margin, underscoring the strong contribution of the improved backbones (Table 4) and the effectiveness of our fusion strategy. The proposed modules then provide additional complementary gains on top of this strong baseline.

4.7.3 VSTR Impact Assessment. The training dataset consists of approximately 32.9% single-person frames, 31.4% two-person frames, and 35.7% frames with more than two persons, indicating a relatively balanced distribution across different interaction complexities. In contrast, the validation dataset is highly imbalanced, with 93.7% of frames containing exactly two persons, while only 4.5% are single-person frames and 1.8% involve more than two persons. Consequently, we extracted a series of representative videos from the validation set to evaluate the effectiveness of the VSTR module. Fig 7 compares the mAP for different video IDs, assessing the model’s performance with and without the integration of VSTR module. The blue bars represent the performance of our proposed method, which includes the VSTR module, while the red bars indicate the performance when the VSTR module is replaced by the corresponding baseline configuration. The comparison clearly indicates that, in most video instances, the incorporation of the VSTR module results in a marked improvement in mAP. For example, in video IDs 1, 3, and 8, the model with VSTR (blue bars) demonstrates a substantial increase in mAP compared to the model without VSTR (red bars). On average, the inclusion of the VSTR module leads to an improvement in mAP by approximately 0.1 to 0.15, underscoring the positive impact of this module on model performance. These findings suggest that the VSTR module plays a critical role in enhancing the model’s ability to accurately detect and classify speakers, particularly in interactive settings with multiple speakers.

4.7.4 PSA Impact Assessment. Fig 8 presents a comparative analysis of mAP and Acc under varying SNR conditions, specifically examining the effects of the PSA encoder. The orange line represents our method, which includes the PSA encoder, while the blue line indicates the performance of the model where the PSA encoder is replaced by the pre-trained Whisper backbone. We observe that under strong noise conditions (when the SNR is negative), Our method significantly outperforms the model that uses only the audio encoder (baseline configuration). For instance, at SNR = -10 dB, the model with the PSA encoder achieves an mAP of approximately 0.72 and an Acc of 0.73, whereas the model following baseline configuration achieves an mAP of about 0.63 and an Acc of 0.65. This demonstrates an improvement of 0.09 in mAP and 0.08 in Acc when the PSA encoder is used, highlighting its effectiveness in mitigating the impact of noise on

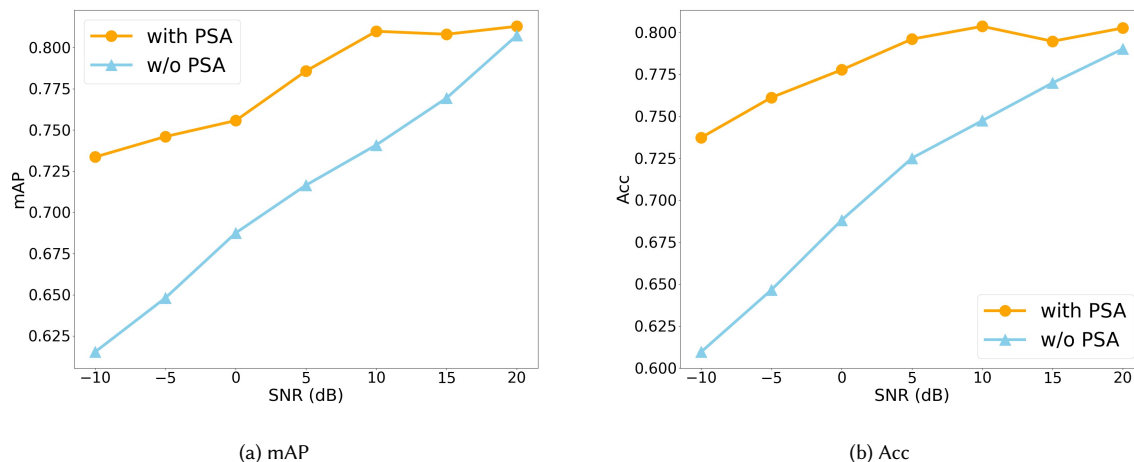


Fig. 8. Comparison of model performance with PSA training and without it (i.e., using the pre-trained Whisper backbone) under different SNR levels.

performance. As the SNR increases, the gap between the two models narrows, but the PSA encoder still consistently provides better performance across all SNR levels, particularly in noisy environments. This analysis underscores the crucial role of the PSA encoder in improving the robustness and Acc of the model under challenging conditions.

4.7.5 VMMA Impact Assessment. Table 5 comprehensively analyzes the effects of different VMMA module settings on the validation set. The results indicate that without VMMA module, the model achieves an Acc of 77.40% and an mAP of 79.37%. When fine-grained VMMA is applied, the model’s performance significantly improves, reaching 81.66% Acc and 84.53% mAP, demonstrating that detailed and precise modality awareness is crucial for optimal results. For coarse-grained VMMA, the adaptive β parameter yields the best performance, achieving an Acc of 81.14% and a mAP of 84.83%. This suggests that utilizing an adaptive threshold allows for optimal handling of modality loss, as it dynamically adjusts based on the data. In comparison, when a fixed threshold of 20% is applied, the performance slightly decreases, with an Acc of 80.29% and an mAP of 84.07%. As the threshold increases to 50% and 70%, further declines are observed, with accuracies of 78.18% and 78.01%, and mAPs of 83.73% and 83.50%, respectively. These findings indicate that the adaptive β is more effective for managing missing data in coarse-grained VMMA, while the fine-grained VMMA method continues to provide the highest overall performance, underscoring the significance of detailed modality handling within the multi-modal framework.

4.8 Qualitative Analysis

This section provides visual examples of the challenging scenarios addressed by EgoAdapt and compares its performance with other state-of-the-art methods. The scenarios include multi-speaker environments, missing visual modalities, and strong background noise, where the model’s ability to handle these difficulties is highlighted.

Figure 9 compares our proposed method with QuAVF [37], the current state-of-the-art method, in a multi-speaker environment where multiple individuals speak simultaneously. The results reveal that existing methods, which do not account for head orientation, often misidentify other individuals in the scene as addressing the camera wearer. In contrast, our method effectively incorporates head orientation, significantly minimizing misidentifications and

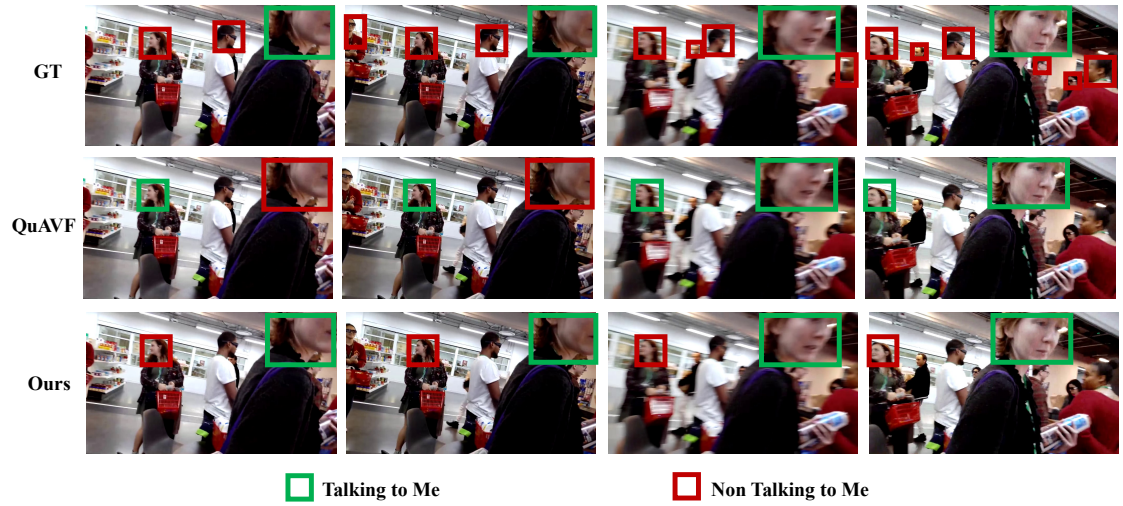


Fig. 9. Comparison of our proposed method with QuAVF [37] (currently the SOTA method) in a multi-speaker environment where multiple individuals are speaking, and the model must correctly identify who is speaking to the camera wearer.

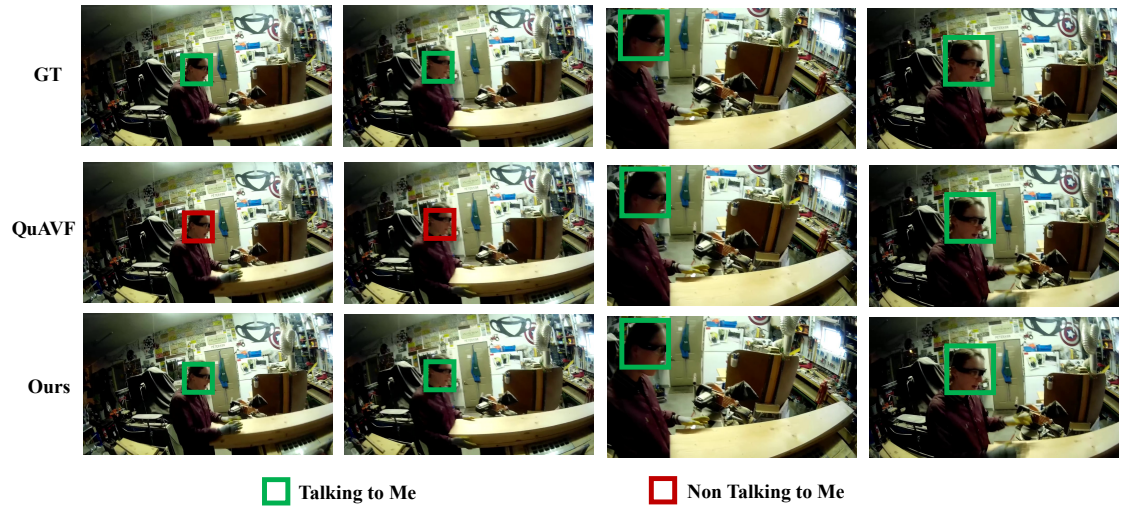


Fig. 10. Comparison of our proposed method with QuAVF [37] in noisy background scenario, where the model must distinguish between relevant and irrelevant audio signals.

accurately identifying who directly engages with the camera wearer. This distinction is vital in complex environments with multiple speakers, where precise interaction analysis is essential.

Figure 10 illustrates a comparison between the performance of our proposed method and QuAVF in a noisy environment. In the first half of the video segment, the speaker is positioned relatively far from the camera wearer, and the noise of the surrounding machinery largely masks the speaker’s voice. As a result, the existing method fails to identify the speaker, leading to misclassification correctly. In contrast, our method accurately identifies the speaker throughout

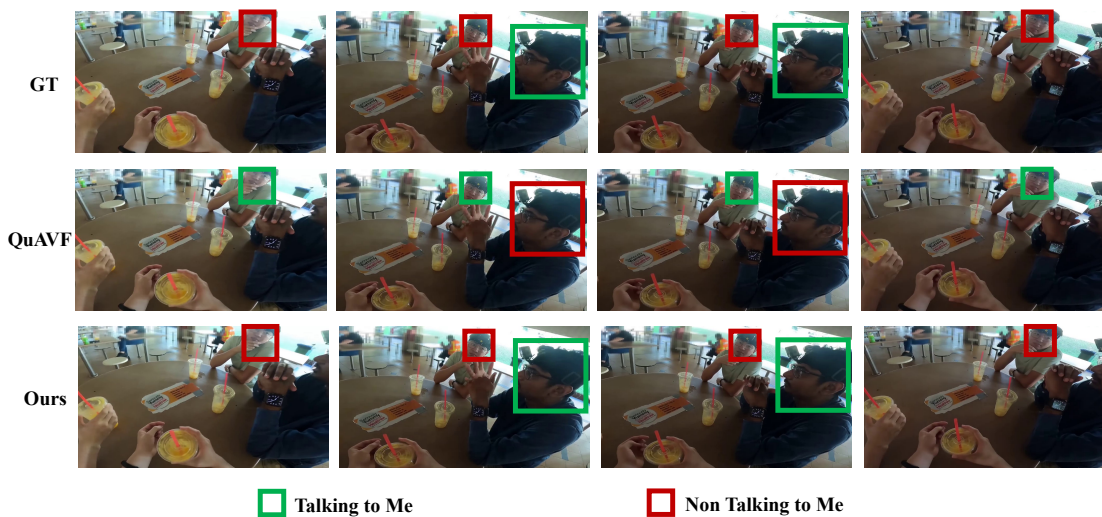


Fig. 11. Comparison of our proposed method with QuAVF [37] in the scenario where the visual modality is partially missing, and the model relies on audio and contextual information to make predictions.

the video, demonstrating robustness against background noise and maintaining correct speaker identification even when environmental sounds partially obscure the audio signal.

Figure 11 compares the results obtained from our proposed method and QuAVF in scenarios where the visual modality is partially absent. Existing methods frequently misidentify a listener—who remains consistently present in the scene—as the individual addressing the camera wearer. This misidentification can occur even when the actual speaker is temporarily occluded due to camera movement. In contrast, our method effectively distinguishes between the speaker and the listener, accurately identifying the correct speaker even in challenging situations where the speaker may be intermittently out of view. This capability is critical for ensuring reliable interaction analysis in dynamic environments.

4.9 Limitations

EgoAdapt assumes temporally synchronized visual and auditory inputs, which may limit its applicability in unconstrained real-world recordings where synchronization is imperfect. The multi-stage attention fusion incurs higher computational cost than simpler fusion schemes, making deployment in resource-limited settings more challenging. Moreover, our experiments are conducted on specific egocentric datasets, and the transferability to other domains remains to be explored in future work.

5 CONCLUSIONS

In this study, we introduced EgoAdapt, an innovative framework designed to enhance the robustness of egocentric interactive speaker detection in scenarios characterized by missing modalities. By leveraging three critical modules—the Visual Speaker Target Recognition (VSTR) module, the Parallel Shared-weight Audio (PSA) encoder, and the Visual Modality Missing Awareness (VMMA) module—EgoAdapt effectively integrates head movements, lip movements, and audio cues. The VSTR module allows for a nuanced understanding of non-verbal cues and verbal cues, enhancing the model’s ability to determine speaker intent accurately. Meanwhile, the PSA encoder enhances the model’s resilience

to noisy environments by improving audio feature extraction under challenging conditions. The VMMA module dynamically assesses the presence or absence of visual information at each frame, allowing EgoAdapt to adapt its reliance on audio or visual cues in real-time. Our comprehensive evaluations on the TTM benchmark of the Ego4D dataset demonstrate that EgoAdapt not only achieves competitive performance but also surpasses existing baseline methods, affirming its effectiveness in robust interactive speaker detection.

References

- [1] R Rashmi Adyapady and BJMS Annappa. 2023. A comprehensive review of facial expression recognition techniques. *Multimedia Systems* 29, 1 (2023), 73–103.
- [2] Harsh Ahlawat, Naveen Aggarwal, and Deepti Gupta. 2025. Automatic Speech Recognition: A survey of deep learning techniques and approaches. *International Journal of Cognitive Computing in Engineering* 6 (2025), 201–237.
- [3] Nefeli Andreou, Andreas Aristidou, and Yiorgos Chrysanthou. 2022. Pose representations for deep skeletal animation. In *Computer Graphics Forum*. Wiley Online Library, 155–167.
- [4] Nefeli Andreou, Andreas Lazarou, Andreas Aristidou, and Yiorgos Chrysanthou. 2021. A hierarchy-aware pose representation for deep character animation. *CoRR* (2021).
- [5] Alexei Baevski, Yuhao Zhou, Abdelrahman Mohamed, and Michael Auli. 2020. wav2vec 2.0: A framework for self-supervised learning of speech representations. *Advances in neural information processing systems* 33 (2020), 12449–12460.
- [6] Aryel Beck, Brett Stevens, Kim A Bard, and Lola Cañamero. 2012. Emotional body language displayed by artificial agents. *ACM Transactions on Interactive Intelligent Systems (TiiS)* 2, 1 (2012), 1–29.
- [7] Jacob Benesty, Shoji Makino, and Jingdong Chen. 2006. *Speech enhancement*. Springer Science & Business Media.
- [8] Mohamed Benzeghiba, Renato De Mori, Olivier Deroo, Stephane Dupont, Teodora Erbes, Denis Jouvet, Luciano Fissore, Pietro Laface, Alfred Mertins, Christophe Ris, et al. 2007. Automatic speech recognition and speech variability: A review. *Speech communication* 49, 10-11 (2007), 763–786.
- [9] Joan-Isaac Biel and Daniel Gatica-Perez. 2011. VlogSense: Conversational behavior and social attention in YouTube. *ACM Transactions on Multimedia Computing, Communications, and Applications (TOMM)* 7, 1 (2011), 1–21.
- [10] Dan Bohus and Alexander I Rudnicky. 2009. The RavenClaw dialog management framework: Architecture and systems. *Computer Speech & Language* 23, 3 (2009), 332–361.
- [11] Antoine Bordes, Y-Lan Boureau, and Jason Weston. 2017. Learning End-to-End Goal-Oriented Dialog. In *International Conference on Learning Representations*.
- [12] Andrew J Calder and Andrew W Young. 2016. Understanding the recognition of facial identity and facial expression. *Facial Expression Recognition* (2016), 41–64.
- [13] Sanyuan Chen, Chengyi Wang, Zhengyang Chen, Yu Wu, Shujie Liu, Zhuo Chen, Jinyu Li, Naoyuki Kanda, Takuya Yoshioka, Xiong Xiao, et al. 2022. Wavlm: Large-scale self-supervised pre-training for full stack speech processing. *IEEE Journal of Selected Topics in Signal Processing* 16, 6 (2022), 1505–1518.
- [14] Yihua Cheng, Haofei Wang, Yiwei Bao, and Feng Lu. 2024. Appearance-based gaze estimation with deep learning: A review and benchmark. *IEEE Transactions on Pattern Analysis and Machine Intelligence* (2024).
- [15] Gourav Datta, Tyler Etchart, Vivek Yadav, Varsha Hedau, Pradeep Natarajan, and Shih-Fu Chang. 2022. Asd-transformer: Efficient active speaker detection using self and multimodal transformers. In *IEEE International Conference on Acoustics, Speech and Signal Processing (ICASSP)*. 4568–4572.
- [16] Xiaohan Ding, Xiangyu Zhang, Ningning Ma, Jungong Han, Guiguang Ding, and Jian Sun. 2021. Repvgg: Making vgg-style convnets great again. In *Proceedings of the IEEE/CVF conference on computer vision and pattern recognition*. 13733–13742.
- [17] Omar Elharrouss, Noor Almaadeed, and Somaya Al-Maadeed. 2021. A review of video surveillance systems. *Journal of Visual Communication and Image Representation* 77 (2021), 103116.
- [18] Yariv Ephraim and Israel Cohen. 2006. Recent advancements in speech enhancement. *The electrical engineering handbook* 35 (2006).
- [19] Gabriele Fanelli, Juergen Gall, and Luc Van Gool. 2011. Real time head pose estimation with random regression forests. In *CVPR 2011*. IEEE, 617–624.
- [20] Gerald Friedland, Chuohao Yeo, and Hayley Hung. 2010. Dialocalization: Acoustic speaker diarization and visual localization as joint optimization problem. *ACM Transactions on Multimedia Computing, Communications, and Applications (TOMM)* 6, 4 (2010), 1–18.
- [21] Huilin Ge, Zhiyu Zhu, Yuewei Dai, Biao Wang, and Xuedong Wu. 2022. Facial expression recognition based on deep learning. *Computer Methods and Programs in Biomedicine* 215 (2022), 106621.
- [22] Kristen Grauman, Andrew Westbury, Eugene Byrne, Zachary Chavis, Antonino Furnari, Rohit Girdhar, Jackson Hamburger, Hao Jiang, Miao Liu, Xingyu Liu, et al. 2022. Ego4d: Around the world in 3,000 hours of egocentric video. In *Proceedings of the IEEE/CVF Conference on Computer Vision and Pattern Recognition*. 18995–19012.
- [23] Meng-Hao Guo, Tian-Xing Xu, Jiang-Jiang Liu, Zheng-Ning Liu, Peng-Tao Jiang, Tai-Jiang Mu, Song-Hai Zhang, Ralph R Martin, Ming-Ming Cheng, and Shi-Min Hu. 2022. Attention mechanisms in computer vision: A survey. *Computational visual media* 8, 3 (2022), 331–368.

- [24] Niels Haering, Péter L Venetianer, and Alan Lipton. 2008. The evolution of video surveillance: an overview. *Machine Vision and Applications* 19, 5 (2008), 279–290.
- [25] Jan-Gerrit Harms, Pavel Kucherbaev, Alessandro Bozzon, and Geert-Jan Houben. 2018. Approaches for dialog management in conversational agents. *IEEE Internet Computing* 23, 2 (2018), 13–22.
- [26] Kaiming He, Xiangyu Zhang, Shaoqing Ren, and Jian Sun. 2016. Deep residual learning for image recognition. In *Proceedings of the IEEE conference on computer vision and pattern recognition*. 770–778.
- [27] Thorsten Hempel, Ahmed A Abdelrahman, and Ayoub Al-Hamadi. 2022. 6d rotation representation for unconstrained head pose estimation. In *IEEE International Conference on Image Processing (ICIP)*. 2496–2500.
- [28] Wei-Ning Hsu, Benjamin Bolte, Yao-Hung Hubert Tsai, Kushal Lakhotia, Ruslan Salakhutdinov, and Abdelrahman Mohamed. 2021. Hubert: Self-supervised speech representation learning by masked prediction of hidden units. *IEEE/ACM transactions on audio, speech, and language processing* 29 (2021), 3451–3460.
- [29] Jie Hu, Li Shen, and Gang Sun. 2018. Squeeze-and-excitation networks. In *Proceedings of the IEEE conference on computer vision and pattern recognition*. 7132–7141.
- [30] Ziyang Jiang, Xueyan Chen, Shuai Wang, Xinyuan Qian, and Haizhou Li. 2025. TPEech: Target Speaker Extraction and Noise Suppression With Historical Dialogue Text Cues. *IEEE Signal Processing Letters* 33 (2025), 351–355.
- [31] Anuradha Kar and Peter Corcoran. 2017. A review and analysis of eye-gaze estimation systems, algorithms and performance evaluation methods in consumer platforms. *IEEE Access* 5 (2017), 16495–16519.
- [32] Sehoon Kim, Amir Gholami, Albert Shaw, Nicholas Lee, Karttikeya Mangalam, Jitendra Malik, Michael W Mahoney, and Kurt Keutzer. 2022. Squeezeformer: An efficient transformer for automatic speech recognition. *Advances in Neural Information Processing Systems* 35 (2022), 9361–9373.
- [33] Martha Larson, Gareth JF Jones, et al. 2012. Spoken content retrieval: A survey of techniques and technologies. *Foundations and Trends® in Information Retrieval* 5, 4–5 (2012), 235–422.
- [34] Lin-shan Lee, James Glass, Hung-yi Lee, and Chun-an Chan. 2015. Spoken content retrieval—beyond cascading speech recognition with text retrieval. *IEEE/ACM Transactions on Audio, Speech, and Language Processing* 23, 9 (2015), 1389–1420.
- [35] Jinyu Li et al. 2022. Recent advances in end-to-end automatic speech recognition. *APSIPA Transactions on Signal and Information Processing* 11, 1 (2022).
- [36] Shan Li and Weihong Deng. 2020. Deep facial expression recognition: A survey. *IEEE transactions on affective computing* 13, 3 (2020), 1195–1215.
- [37] Hsi-Che Lin, Chien-Yi Wang, Min-Hung Chen, Szu-Wei Fu, and Yu-Chiang Frank Wang. 2023. QuAVF: Quality-aware Audio-Visual Fusion for Ego4D Talking to Me Challenge. *arXiv preprint arXiv:2306.17404* (2023).
- [38] Tao Liu, Mingyang Zhang, Zhihao Li, Hanjie Dou, Wangyang Zhang, Jiaqian Yang, Pengfan Wu, Dongxiao Li, and Xiaojing Mu. 2025. Machine learning-assisted wearable sensing systems for speech recognition and interaction. *Nature Communications* 16, 1 (2025), 2363.
- [39] Yi Luo, Cong Han, Nima Mesgarani, Enea Ceolini, and Shih-Chii Liu. 2019. FaSNet: Low-latency adaptive beamforming for multi-microphone audio processing. In *IEEE automatic speech recognition and understanding workshop (ASRU)*. 260–267.
- [40] Yi Luo and Nima Mesgarani. 2018. Tasnet: time-domain audio separation network for real-time, single-channel speech separation. In *2018 IEEE International Conference on Acoustics, Speech and Signal Processing (ICASSP)*. IEEE, 696–700.
- [41] Yi Luo and Nima Mesgarani. 2019. Conv-tasnet: Surpassing ideal time–frequency magnitude masking for speech separation. *IEEE/ACM transactions on audio, speech, and language processing* 27, 8 (2019), 1256–1266.
- [42] Mishaim Malik, Muhammad Kamran Malik, Khawar Mehmood, and Imran Makhdoom. 2021. Automatic speech recognition: a survey. *Multimedia Tools and Applications* 80, 6 (2021), 9411–9457.
- [43] Laura Martinez, Virginia B Falvello, Hillel Aviezer, and Alexander Todorov. 2016. Contributions of facial expressions and body language to the rapid perception of dynamic emotions. *Cognition and Emotion* 30, 5 (2016), 939–952.
- [44] Ian McLoughlin. 2009. *Applied speech and audio processing: with Matlab examples*. Cambridge University Press.
- [45] Gregory P Meyer, Shalini Gupta, Iuri Frosio, Dikpal Reddy, and Jan Kautz. 2015. Robust model-based 3d head pose estimation. In *Proceedings of the IEEE international conference on computer vision*. 3649–3657.
- [46] Erik Murphy-Chutorian and Mohan Manubhai Trivedi. 2008. Head pose estimation in computer vision: A survey. *IEEE transactions on pattern analysis and machine intelligence* 31, 4 (2008), 607–626.
- [47] Xinyuan Qian, Jiaran Gao, Yaodan Zhang, Qiquan Zhang, Hexin Liu, Leibny Paola Garcia, and Haizhou Li. 2025. SAV-SE: Scene-aware Audio-Visual Speech Enhancement with Selective State Space Model. *IEEE Journal of Selected Topics in Signal Processing* (2025).
- [48] Xinyuan Qian, Hao Tang, Jichen Yang, Hongxu Zhu, and Xu-Cheng Yin. 2025. Dual-path transformer-based gan for co-speech gesture synthesis. *International Journal of Social Robotics* 17, 10 (2025), 2065–2076.
- [49] Alec Radford, Jong Wook Kim, Chris Hallacy, Aditya Ramesh, Gabriel Goh, Sandhini Agarwal, Girish Sastry, Amanda Askell, Pamela Mishkin, Jack Clark, et al. 2021. Learning transferable visual models from natural language supervision. In *International Conference on Machine Learning*. 8748–8763.
- [50] Rajeev Ranjan, Vishal M Patel, and Rama Chellappa. 2017. Hyperface: A deep multi-task learning framework for face detection, landmark localization, pose estimation, and gender recognition. *IEEE transactions on pattern analysis and machine intelligence* 41, 1 (2017), 121–135.
- [51] Razieh Rastgoo, Kourosh Kiani, Sergio Escalera, Vassilis Athitsos, and Mohammad Sabokrou. 2024. A survey on recent advances in Sign Language Production. *Expert Systems with Applications* 243 (2024), 122846.

- [52] Siti Nur Aisyah Mohd Robi, Muhammad Atiff Zakwan Mohd Ariffin, Mohd Azri Mohd Izhar, Norulhusna Ahmad, and Hazilah Mad Kaidi. 2024. Active speaker detection using audio, visual, and depth modalities: A survey. *IEEE Access* 12 (2024), 96617–96634.
- [53] Nataniel Ruiz, Eunji Chong, and James M Rehg. 2018. Fine-grained head pose estimation without keypoints. In *Proceedings of the IEEE conference on computer vision and pattern recognition workshops*. 2074–2083.
- [54] Helmer Strik and Catia Cucchiari. 1999. Modeling pronunciation variation for ASR: A survey of the literature. *Speech Communication* 29, 2-4 (1999), 225–246.
- [55] Cem Subakan, Mirco Ravanelli, Samuele Cornell, Mirko Bronzi, and Jianyuan Zhong. 2021. Attention is all you need in speech separation. In *IEEE International Conference on Acoustics, Speech and Signal Processing (ICASSP)*. 21–25.
- [56] Richard Szeliski. 2022. *Computer vision: algorithms and applications*. Springer Nature.
- [57] Ruijie Tao, Zexu Pan, Rohan Kumar Das, Xinyuan Qian, Mike Zheng Shou, and Haizhou Li. 2021. Is someone speaking? exploring long-term temporal features for audio-visual active speaker detection. In *Proceedings of the 29th ACM International Conference on Multimedia*. 3927–3935.
- [58] Ruijie Tao, Xinyuan Qian, Rohan Kumar Das, Xiaoxue Gao, Jiadong Wang, and Haizhou Li. 2025. Enhancing Real-World Active Speaker Detection With Multi-Modal Extraction Pre-Training. *IEEE Transactions on Multimedia* 27 (2025), 2362–2373. doi:10.1109/TMM.2024.3521791
- [59] Zhan Tong, Yibing Song, Jue Wang, and Limin Wang. 2022. Videomae: Masked autoencoders are data-efficient learners for self-supervised video pre-training. *Advances in neural information processing systems* 35 (2022), 10078–10093.
- [60] Minh Tran, Yelin Kim, Che-Chun Su, Cheng-Hao Kuo, Min Sun, and Mohammad Soleymani. 2025. Ex2Eg-MAE: A Framework for Adaptation of Exocentric Video Masked Autoencoders for Egocentric Social Role Understanding. In *Computer Vision – ECCV 2024*, Aleš Leonardis, Elisa Ricci, Stefan Roth, Olga Russakovsky, Torsten Sattler, and Gül Varol (Eds.). Springer Nature Switzerland, Cham, 1–19.
- [61] Vassilios Tsakanikas and Tasos Dagiuklas. 2018. Video surveillance systems-current status and future trends. *Computers & Electrical Engineering* 70 (2018), 736–753.
- [62] Athanasios Voulodimos, Nikolaos Doulamis, Anastasios Doulamis, and Eftychios Protopapadakis. 2018. Deep learning for computer vision: A brief review. *Computational intelligence and neuroscience* 2018, 1 (2018), 7068349.
- [63] DeLiang Wang and Jitong Chen. 2018. Supervised speech separation based on deep learning: An overview. *IEEE/ACM Transactions on Audio, Speech, and Language Processing* 26, 10 (2018), 1702–1726.
- [64] DeLiang Wang and Jitong Chen. 2018. Supervised speech separation based on deep learning: An overview. *IEEE/ACM transactions on audio, speech, and language processing* 26, 10 (2018), 1702–1726.
- [65] Dong Wang, Xiaodong Wang, and Shaohe Lv. 2019. An overview of end-to-end automatic speech recognition. *Symmetry* 11, 8 (2019), 1018.
- [66] Jiadong Wang, Xinyuan Qian, and Haizhou Li. 2024. Predict-and-update network: Audio-visual speech recognition inspired by human speech perception. *IEEE/ACM Trans. on Audio, Speech, and Language Processing* (2024).
- [67] Jian-Gang Wang and Eric Sung. 2002. Study on eye gaze estimation. *IEEE Transactions on Systems, Man, and Cybernetics, Part B (Cybernetics)* 32, 3 (2002), 332–350.
- [68] Xinming Wang, Jianhua Zhang, Hanlin Zhang, Shuwen Zhao, and Honghai Liu. 2021. Vision-based gaze estimation: A review. *IEEE Transactions on Cognitive and Developmental Systems* 14, 2 (2021), 316–332.
- [69] Gordon Wichern, Joe Antognini, Michael Flynn, Licheng Richard Zhu, Emmett McQuinn, Dwight Crow, Ethan Manilow, and Jonathan Le Roux. 2019. WHAM!: Extending Speech Separation to Noisy Environments. *Interspeech 2019* (2019).
- [70] Junwen Xiong, Yu Zhou, Peng Zhang, Lei Xie, Wei Huang, and Yufei Zha. 2022. Look&listen: Multi-modal correlation learning for active speaker detection and speech enhancement. *IEEE Transactions on Multimedia* (2022).
- [71] Junwen Xiong, Yu Zhou, Peng Zhang, Lei Xie, Wei Huang, and Yufei Zha. 2023. Look&listen: Multi-Modal Correlation Learning for Active Speaker Detection and Speech Enhancement. *IEEE Transactions on Multimedia* 25 (2023), 5800–5812. doi:10.1109/TMM.2022.3199109
- [72] Linfeng Xu, Qingbo Wu, Lili Pan, Fanman Meng, Hongliang Li, Chiyuan He, Hanxin Wang, Shaoxu Cheng, and Yu Dai. 2024. Towards Continual Egocentric Activity Recognition: A Multi-Modal Egocentric Activity Dataset for Continual Learning. *IEEE Transactions on Multimedia* 26 (2024), 2430–2443. doi:10.1109/TMM.2023.3295899
- [73] Zihui Xue, Yale Song, Kristen Grauman, and Lorenzo Torresani. 2023. Egocentric video task translation. In *Proceedings of the IEEE/CVF Conference on Computer Vision and Pattern Recognition*. 2310–2320.
- [74] Dong Yu and Lin Deng. 2016. *Automatic speech recognition*. Vol. 1. Springer.
- [75] Xucong Zhang, Yusuke Sugano, Mario Fritz, and Andreas Bulling. 2015. Appearance-based gaze estimation in the wild. In *Proceedings of the IEEE conference on computer vision and pattern recognition*. 4511–4520.
- [76] Yuanhang Zhang, Susan Liang, Shuang Yang, Xiao Liu, Zhongqin Wu, and Shiguang Shan. 2021. Ictcas-ucas-tal submission to the ava-activespeaker task at activitynet challenge 2021. *The ActivityNet Large-Scale Activity Recognition Challenge* 1, 3 (2021), 4.
- [77] Yi Zhou, Connelly Barnes, Jingwan Lu, Jimei Yang, and Hao Li. 2019. On the continuity of rotation representations in neural networks. In *Proceedings of the IEEE/CVF conference on computer vision and pattern recognition*. 5745–5753.
- [78] Xiangyu Zhu, Zhen Lei, Xiaoming Liu, Hailin Shi, and Stan Z Li. 2016. Face alignment across large poses: A 3d solution. In *Proceedings of the IEEE conference on computer vision and pattern recognition*. 146–155.
- [79] Udo Zölzer. 2022. *Digital audio signal processing*. John Wiley & Sons.